Catalysis Surveys from Asia, Vol. 9, No. 4, December 2005 (© 2006)
DOI: 10.1007/s10563-005-9157-0

Photocatalytic water splitting under visible light with particulate semiconductor catalysts

Jae Sung Lee*

Department of Chemical Engineering, Pohang University of Science and Technology (POSTECH), San 31 Hyoja-dong, Pohang 790–784, Republic of Korea

Photocatalytic water splitting (PWS) is the most promising technology to produce H_2 energy directly from renewable water and solar light. PWS has made a remarkable progress last decades under ultra-violet (UV) light, but there are many technical challenges remaining for PWS under visible light. Several approaches are taken in search of photocatalysts efficient for PWS under visible light: (i) to find new single phase materials, (ii) to decorate UV-active photocatalysts with a photosensitizer absorbing visible light, (iii) to tune the band gap energy by modifying cations or anions of UV-active photocatalysts with substitutional doping, and (iv) to fabricate multi-component photocatalysts by forming composites or solid solutions. This article discusses the above approaches based on our experimental results as well as data available in the literature. At the moment, the greatest challenge to the progress of visible light PWS is the low efficiency of light utilization. Finding new photocatalytic materials with unique structure and phase is still the key to the success. In addition, the synthesis of these materials with high crystallinity and high surface area is also important, because these properties exert great impact on the activity of the material of the same structure and phase. Finally, smart combination and modification of known materials could also be fruitful.

KEY WORDS: photocatalysts; water splitting; visible light; metal doping; nitrogen-doping; composite.

1. Introduction

Hydrogen is expected to become the main energy carrier of the future because of its high-energy capacity and environmental friendliness. Hydrogen will be produced from fossil fuels by established technologies in the near future, but eventually it should be manufactured from a renewable energy source such as solar energy. Photocatalytic water splitting (PWS) is the most promising technology for the purpose, since H_2 could be obtained directly from abundant and renewable water and solar light from the process. If successfully developed with economic viability, this could be the ultimate technology that could solve both energy and environmental problems altogether in the future. Since its demonstration by Fujishima and Honda in 1972 over a TiO_2 single crystal electrode [1], PWS has made a remarkable progress last decades under ultra-violet (UV) light [2–4].

We also have reported that (110) layered perovskite materials, a series of homologous structures with a generic composition of $A_mB_mO_{3m+2}$ ($m = 4$, 5; A = Ca, Sr, La; B = Nb, Ti, Ta) are highly active photocatalysts that promote overall water splitting into a stoichiometric mixture of H_2 and O_2 (2:1 by volume) under UV light [5–13]. Unlike the more common (100) layered perovskite materials [2,14,15], our materials have layers parallel to (110) surface of the perovskite structure. Furthermore, the materials are 'highly donor-doped' [16] since a pentavalent element substitutes for the tetravalent Ti, or a trivalent element substitutes for the divalent Ca in the original perovskite structure, $CaTiO_3$. At the moment, the state-of-the-art photocatalysts such as La-doped $NaTaO_3$ [17] and Ba-doped $Sr_2Nb_2O_7$ [13], can produce a stoichiometric mixture of H_2 and O_2 from water under UV light with quantum yields (the percentage of absorbed photons that have been used to produce H_2 and O_2) as high as ca. 50%.

These exciting developments in UV photocatalysis have unfortunately a limited value for the practical, large-scale hydrogen manufacture, because the solar spectrum contains only ca. 4% of UV light. Visible light is far more abundant (ca. 46%) and thus a more useful region in the solar spectrum. The development of visible light photocatalysts, therefore, has become an important topic in the photocatalysis research today. The PWS under visible light has been a great challenge once called 'the Holy Grail of Chemistry', yet there has been significant progress in recent years that suggests that it could indeed become a viable energy conversion technology in near future. The present article reviews the development of visible-light photocatalysts active for water splitting. Although the current status and perspective of the technology in general are discussed, the primary focus of discussion in this particular article is given to our own results. Only a limited number of directly related works in the literature will be discussed. Excellent reviews of the similar scope describing the activity of other laboratories have also been published [17,18].

* To whom correspondence should be addressed.
E-mail: jlee@postech.ac.kr

1571-1013/05/0217–0227/0

2. Photocatalytic water splitting under visible light

PWS, like other photocatalytic processes, is initiated when a semiconductor photocatalyst absorbs photons with energies greater than its band gap energy. This absorption creates excited photoelectrons in the conduction band and holes in the valence band of the semiconductor as schematically shown in figure 1. The photoelectrons and holes reduce and oxidize water to produce the stoichiometric 2:1 mixture of H_2 and O_2 by the following reactions:

$$\text{Oxidation: } H_2O + 2h^+ \rightarrow 2H^+ + \frac{1}{2}O_2 \quad (1)$$

$$\text{Reduction: } 2H^+ + 2e^- \rightarrow H_2 \quad (2)$$

$$\text{Overall reaction: } H_2O \rightarrow H_2 + \frac{1}{2}O_2 \quad (3)$$

The overall reaction is a four-electron transfer reaction (per O_2 molecule) and usually promoted by metal or metal oxide co-catalysts (denoted as cat 1 and cat 2 in figure 1) deposited on the semiconductor surfaces. These co-catalysts are known to collect charge carriers and provide catalytic reaction sites for these reactions [19]. The reaction involves the standard Gibbs free energy change ΔG^o of 237 kJ/mol or 1.23 eV. Therefore, any semiconductor photocatalyst should possess a band gap energy (E_g) greater than 1.23 eV to be used for water splitting. In order to be excited by the visible light irradiation, however, its value should be less than ca. 3.0 eV. In addition, the band position of the photocatalyst is also important. For the facile electron and hole transfer, the conduction band should be located at a potential more negative than the reduction potential of water, while the valence band should be located at more positive position than oxidation potential of water as indicated in figure 1. Therefore, the photocatalytic materials for visible light water splitting should satisfy these two requirements of proper band gap energy ($1.23\ \text{eV} < E_g < 3.0\ \text{eV}$) and band positions.

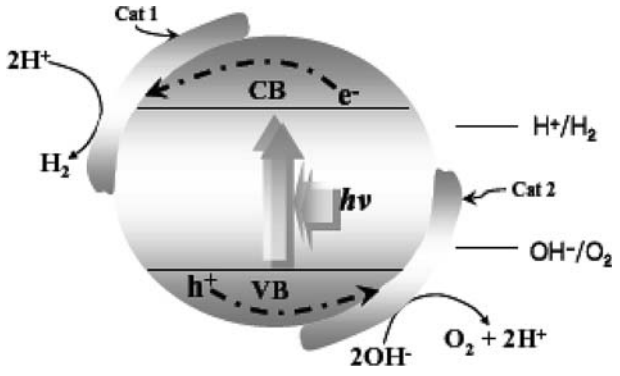

Figure 1. The principle of photocatalytic water splitting. Note that the bottom of the conduction band should be located more negative than the water reduction potential, whereas the top of the valence band more positive than the water oxidation potential.

There are only a limited number of known materials that could satisfy these requirements. For example, chalcogenides such as CdS (2.4 eV) and CdSe (1.7 eV) have ideal band gap energies and band positions for the oxidation and reduction of water molecules under visible light [20,21]. Unfortunately, they are easily corroded in water under irradiation, i.e. CdS itself is oxidized into Cd^{2+} and S^{2-} by the hole produced in its valence band. Thus, we need new materials that are active, stable, and cost-effective in order to make PWS a viable option for hydrogen energy production.

There are several common approaches that are taken in search of photocatalysts for PWS under visible light irradiation: (i) to find new single phase materials, (ii) to decorate UV-active photocatalysts with a photosensitizer absorbing visible light, (iii) to tune the band gap energy by modifying cations or anions of UV-active photocatalysts with substitutional doping, and (iv) to fabricate multi-component photocatalysts by forming composites. This article discusses the above approaches based on our experimental results, except the second approach which was successfully applied for dye-sensitized solar cells [22], but was found to be unstable under PWS conditions.

3. Modification of UV-active photocatalysts by cation doping

The creation of the visible light response by doping a transition metal ions into wide-bandgap, UV-responding photocatalysts has been known for a long time. Examples include V-, Fe- or Cr-doped TiO_2 [23,24], Cr/Sb-doped $SrTiO_3$[25] and Ni-doped InTaO4 [26]. We also have studied Cr- or Fe-doped $La_2Ti_2O_7$ [27,28]. $La_2Ti_2O_7$ is a layered perovskite that showed high activity under UV light for overall PWS [8,9,13] and CH_3Cl decomposition [29].

In order to understand the effect Fe or Cr doping, the electronic band structures of unsubstituted and Cr-substituted $La_2Ti_2O_7$ (for a fictitious composition of $La_2Cr_{0.5}Ti_{1.5}O_7$) were calculated with the Wien 97 code based on the density functional theory. As shown in figure 2a, the edge position and shape of both valence band and conduction band were not affected by substitution of Cr for Ti. The most significant feature in the band structure of Cr-doped $La_2Ti_2O_7$ was the formation of a new band near 1.8–2.3 eV. This localized band formed in the original band gap of $La_2Ti_2O_7$ came from Cr 3d orbital as shown in figure 2b. The figure 2b also indicated small contributions of oxygen and Ti, and essentially no contribution of La to the formation of this interband. The contribution of unoccupied Cr 3d orbital to the conduction band was comparable to that of Ti 3d (figure 2c), while the occupied Cr 3d orbital contributed

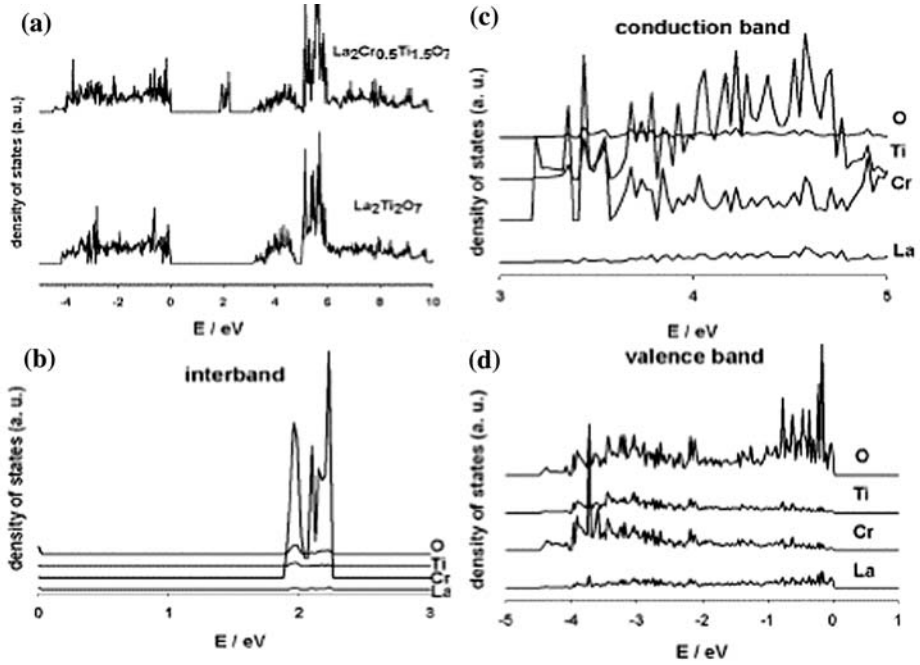

Figure 2. Electronic band structure of Cr-doped $La_2Ti_2O_7$ calculated by the Wien 97 code based on the FLAPW (Full Potential Linearized Augmented Plane Wave) method which used the generalized gradient approximation (GGA), an improvement of the local spin density approximation (LSDA) within the density functional theory.

mainly to the lower energy part of the valence band (figure 2d). The conduction band of $La_2Ti_2O_7$ consisted mainly of the unoccupied Ti 3d orbital, especially in the lower energy region (3–5 eV), and thus the contribution of the unoccupied Cr 3d orbital to the conduction band was substantial for $La_2Cr_{0.5}Ti_{1.5}O_7$.

The UV–Vis absorption property of Cr- or Fe-doped $La_2Ti_2O_7$ was compared in figure 3a. Because of the doping, visible light absorption above 400 nm was created as indicated by the shoulders in absorption spectra. This visible light absorption is due to the excitation of the electrons in the Cr 3d or Fe 3d band to the conduction band as schematically represented in figure 3b. The band gap transition does not take place under visible light due to the wide band gap of $La_2Ti_2O_7$ (3.2 eV).

Photocatalytic activity was measured for pure water under UV light (>200 nm), and in the presence of methanol as a sacrificial hole scavenger under visible light irradiation with a cut-off filter (>420 nm). To promote the hydrogen generation Cr-doped $La_2Ti_2O_7$ (Cr/La = 0.01) was loaded with 1.0 wt% Pt. Under UV irradiation, the photocatalytic activity of Cr- or Fe-doped $La_2Ti_2O_7$ was lower than that of undoped one. As dopant concentration was increased, the activity was lowered further. For undoped $La_2Ti_2O_7$, electrons in the conduction band excited from valence band under UV irradiation could be utilized to produce H_2 and O_2 from *overall* splitting of pure water. According to the band structure calculation of Cr-doped $La_2Ti_2O_7$ shown in figure 2, the major effect of Cr doping was the formation

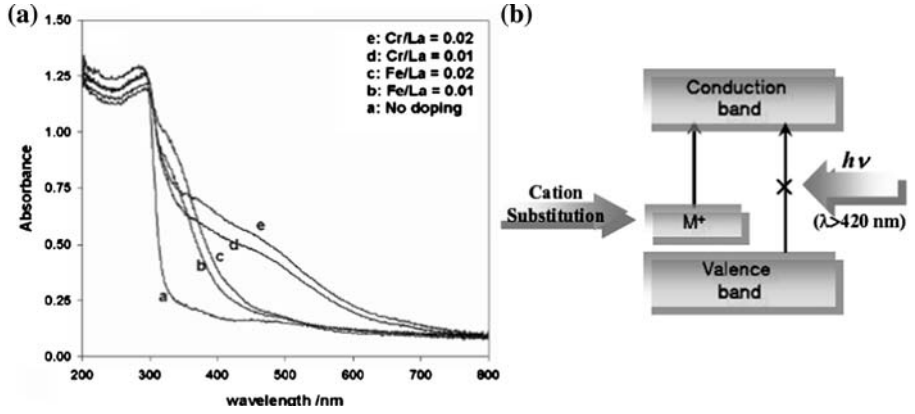

Figure 3. UV–Vis diffuse reflectance spectra of metal (Fe, Cr)-doped $La_2Ti_2O_7$ samples (a) and their band structure model (b). The visible light absorption takes place due to the transition from the interband to the conduction band. The band gap transition does not take place under visible light due to the wide band gap of $La_2Ti_2O_7$ (3.2 eV).

of an interband in the band gap. Under UV irradiation, the electrons in the interband as well as the electrons in the valence band could be excited to the conduction band, resulting in the holes in both the interband and valence band. However, water molecule could not be oxidized by the holes in the interband due to the lower oxidation potential than that required for water oxidation, and thus the new interband could not contribute to the water-splitting activity. Instead, it could serve as a recombination site for photo-generated electrons and holes, which resulted in the lower activity of Cr- or Fe-doped $La_2Ti_2O_7$. Under visible light irradiation, no activity was observed when only pure water was used as reactant. Continuous H_2 evolution was observed when CH_3OH was added as a hole scavenger. The continuous formation of CO_2 also occurs from methanol oxidation by holes. For the same dopant concentration, H_2 evolution rate was a little higher for Cr-doped $La_2Ti_2O_7$ than that for Fe-doped one, which resulted from the difference in the amount of visible light absorption as shown in figure 3a. As the dopant concentration was increased, the activity was decreased for both catalysts, although the amounts of visible light absorption were larger for catalysts with higher dopant concentrations. This is ascribed to the reduced crystallinity of $La_2Ti_2O_7$, which is highly dependent on the dopant concentration, as demonstrated by XRD results (not shown here).

Thus when a wide band gap semiconductor is doped with a transition metal ion, visible light absorption and visible light photocatalytic activity are induced by interband formation in the band gap of the original semiconductor. However, the induced visible light activity is rather low. One reason of the low activity might be the small amount of absorption as indicated by their absorption spectra that show small shoulders in the visible light region instead of total red shift of absorption edge. Attempts to increase the absorption by increasing the doping level usually fail because the original structure is disturbed by excessive doping [27]. An apparent exception is when the doping is made by ion implantation studied extensively by Anpo and coworkers, which induces clean red-shift of the whole absorption edge into the visible light region [24]. But this preparation method involves highly expensive ion implantation equipment. Another limitation is that these substituted sites, albeit responsible for the visible light activity, could also become the sites for energy-wasteful electron–hole recombination and reduce the photocatalytic activity as demonstrated in table 1 under UV light.

4. Modification of UV-active photocatalysts by anion doping

In another approach of modification of UV-active photocatalysts, nitrogen or carbon is doped replacing a part of oxygen. Thus, nitrogen- or carbon-doped TiO_2 are visible light-responding photocatalysts for degradation of organic materials [30] or water splitting [31]. Similarly, TaON, $SrNbO_2N$ and $LaTiO_2N$, perovskite-type oxynitrides, were found to be active for water splitting under visible light irradiation [32–34]. In particular, TaON showed a surprisingly high initial quantum yield of ca. 34% for oxygen evolution from water containing $AgNO_3$ as a sacrificial electron acceptor, although the quantum yield for hydrogen production in the presence of methanol was merely 0.2% [32]. TaON, $SrNbO_2N$ and $LaTiO_2N$ are not doped materials, but compound photocatalysts. Yet, they are discussed here because the involved principle of visible light absorption is the same as discussed below. It was reported that the top of the valence band of oxynitrides consist primarily of N 2p orbitals hybridized with O 2p orbitals, and this yields smaller band-gap energy than pure oxides [30]. This idea forms a good basis to obtain visible light active photocatalysts.

We studied photocatalytic water splitting using nitrogen-doped $Sr_2Nb_2O_7$ under visible light irradiation [35]. This $Sr_2Nb_2O_7$ is also an efficient (110) layered perovskite photocatalyst for overall water splitting showing quantum yields as high as 23% under UV light irradiation [5,6]. $Sr_2Nb_2O_{7-x}N_x$ ($x = 1.47 \sim 2.828$) catalysts were synthesized from a $Sr_2Nb_2O_7$ precursor by nitridation with NH_3 at high temperatures. Thus, a $Sr_2Nb_2O_7$ sample was treated in flowing NH_3 at increasing temperatures from 973 to 1273 K. As the nitridation temperature was increased, the crystal structure transformed from $Sr_2Nb_2O_7$ to its oxynitride, $SrNbO_2N$. The intensity of diffraction peaks of the $Sr_2Nb_2O_7$ phase decreased with the nitriding temperature and later completely disappeared at 1223 K. Figure 4a shows UV–Vis diffuse reflectance (DR) spectra of pure oxide and N-doped samples prepared at increasing nitriding temperatures from 973 to 1273 K. The increase in nitridation temperature shifted the photon absorption of the photocatalysts into visible range. The pure oxide showed the absorption only in UV region (< 300 nm), whereas in nitrided samples, a shoulder started appearing around $\sim$350 nm. This shoulder showed increased intensity and became broader with nitridation temperature, thereby red-shifting the photocatalyst absorption into visible region. From these spectra, straightforward observation of band edge position indicates that experimental band gap would lie in the range of 320–610 nm.

Pt (3.0 wt%)-loaded $Sr_2Nb_2O_{7-x}N_x$ samples showed H_2 evolution for the photocatalytic reduction of water containing methanol as a hole scavenger under visible light irradiation ($\lambda > 400$ nm). Since undoped $Sr_2Nb_2O_7$ did not produce hydrogen under visible light irradiation, it has been demonstrated that N-doping of $Sr_2Nb_2O_7$ induces photocatalytic activity in visible light region. As shown in figure 4b, photocatalytic activity for H_2 evolution showed the maximum at the nitriding temperature of 1073 K. This activity trend was not consistent

Table 1
Photocatalytic activity of metal-doped $La_2Ti_2O_7$

Photocatalysts	Activity (μmol H_2/h)	
	UV irradiation[a] ($\lambda > 200$ nm)	Visible light irradiation[b] ($\lambda > 420$ nm)
$La_2Ti_2O_7$	120	0
Cr–$La_2Ti_2O_7$ (Cr/La = 0.01)	90	15
Cr, Sb-$La_2Ti_2O_7$ (Cr/La = 0.01)	70	4
Cr–$La_2Ti_2O_7$ (Cr/La = 0.05)	50	8
Fe–$La_2Ti_2O_7$ (Fe/La = 0.01)	45	10
Fe–$La_2Ti_2O_7$ (Fe/La = 0.05)	32	5

[a]Measured in an inner irradiation quartz reaction cell under irradiation from a 450 W high pressure Hg lamp; H_2O 500 ml, catalyst 1.0 g.
[b]Measured in outer irradiation cell from 500 W high-pressure Hg lamp; H_2O 100 ml + MeOH 50 ml, catalyst 0.5 g, 420 nm cut-off filter was used. 1 wt% of Pt was loaded using H_2PtCl_6 by photoplatinization.

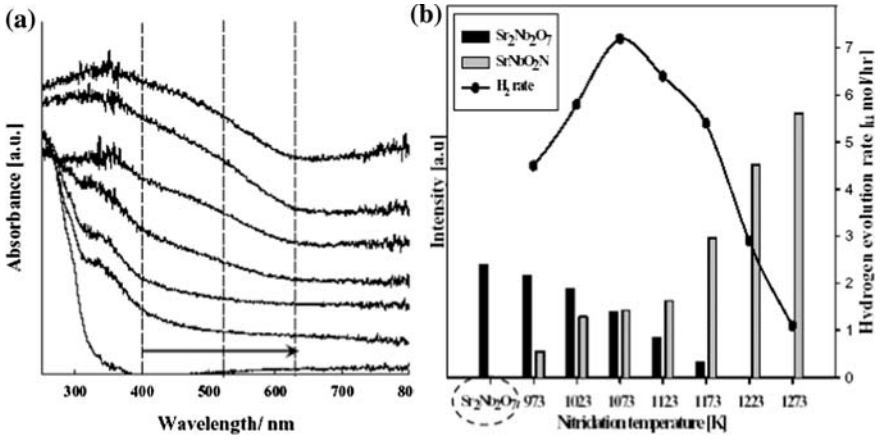

Figure 4. (a) UV–Vis diffuse reflectance spectra of $Sr_2Nb_2O_7$ (bottom) and nitrogen-doped $Sr_2Nb_2O_7$ prepared by NH_3 treatments at increasing temperatures from 973 to 1273 K (towards the top). (b) Hydrogen evolution rates and the XRD peak intensities of $Sr_2Nb_2O_7$ and $SrNbO_2N$ in the samples prepared at various nitridation temperatures.

with variables such as surface area, nitrogen content and crystallinity of the catalyst (not shown). The figure 4b also shows the graph of XRD peak intensity of $Sr_2Nb_2O_7$ ($2\theta = 29.18$) and of $SrNbO_2N$ ($2\theta = 31.22$) versus nitridation temperatures. The maximum rate of H_2 gas evolution is observed when the major phase of the photocatalyst changes from $Sr_2Nb_2O_7$ to $SrNbO_2N$. Thus the structure of the photocatalyst appears to be the most important parameter determining the photocatalytic activity of water decomposition over this type of catalysts. The most active phase is an intermediate phase still maintaining the original layered perovskite structure, but with its oxygen replaced partly with nitrogen to the greatest possible extent. It has been demonstrated that layered structure-type materials have higher activity for water splitting than unlayered structure-type materials of the same composition [13]. An excess N-doping facilitates the collapse of the layered structure of parent oxide ($Sr_2Nb_2O_7$) and turns it into unlayered $SrNbO_2N$. This could rationalize the reduction of activity above 1073 K in figure 4b. The increase of activity below 1073 K is rationalized by the reduction of band gap energy by nitrogen doping. The more nitrogen was doped, the smaller the band gap energy of sample became and greater portion of visible light is absorbed by the photocatalyst.

In order to understand the effect of N doping on $Sr_2Nb_2O_7$, we performed the band structure calculations on pure $Sr_2Nb_2O_7$, N-doped $Sr_2Nb_2O_7$, and the oxynitride $SrNbO_2N$. Figure 5 shows the total and projected partial densities of states for $Sr_2Nb_2O_7$, $Sr_2Nb_2O_5N_2$, and $SrNbO_2N$, where the top of the valence band was set to 0 eV. Also shown as insets are structure models that these calculations are based on. The intermediate was assumed to be $Sr_2Nb_2O_5N_2$, which had the layered perovskite structure identical to the structure of $Sr_2Nb_2O_7$, but its fundamental structural unit making perovskite slabs was $NbO_{6-x}N_x$ octahedrons instead of NbO_6 octahedrons. In the oxynitride, the layered structure is collapsed to form a bulk, cubic phase.

Upon nitrogen doping, the band gap energy is reduced. The states at the top of the valence band for $Sr_2Nb_2O_7$ comes from O 2p orbitals, while the states at conduction band minimum are predominantly contribution of Nb 4d. The contribution from Sr 4d is mainly

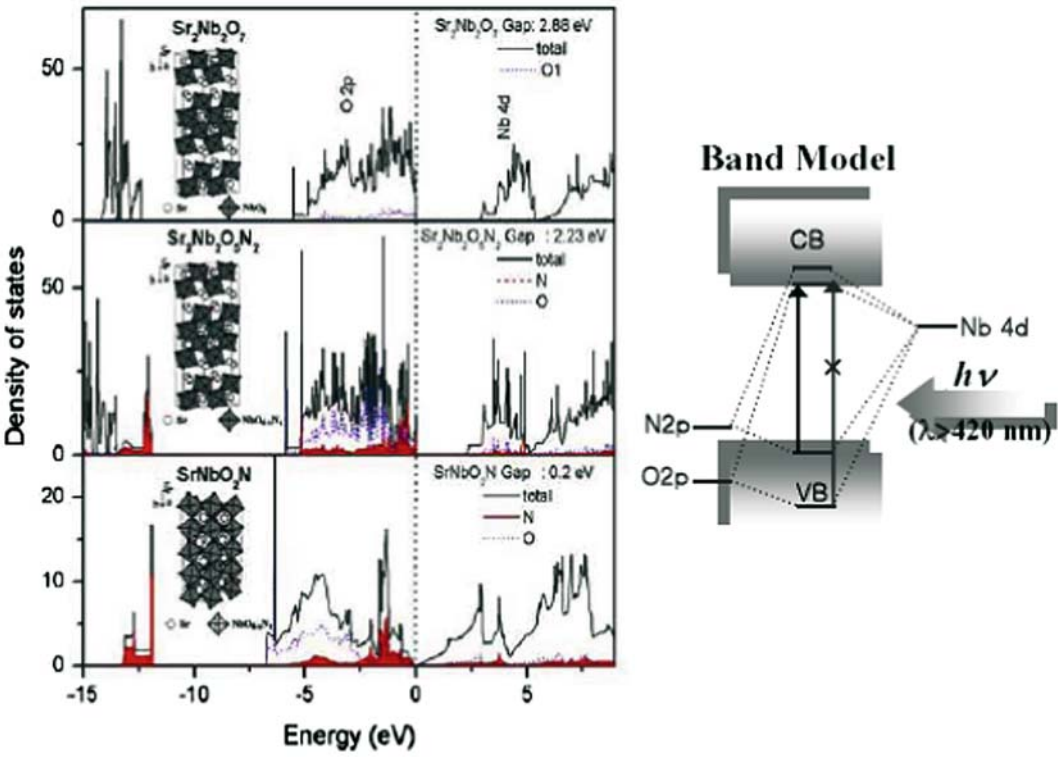

Figure 5. Calculated total and projected density of states of $Sr_2Nb_2O_7$, nitrogen-doped $Sr_2Nb_2O_7$ and $SrNbO_2N$ and their structure models in the inset. The shaded areas are contributions from nitrogen 2p orbital. A band model of nitrogen doped $Sr_2Nb_2O_7$ shows mixing of N 2p (gray area) with O 2p states near the top of the valence band, which causes band gap narrowing and visible light absorption.

directed to conduction band far from its minimum. The main difference observable in nitrogen-doped oxide is that major contribution on the top of valence band comes from N 2p. It is clear from DOS studies that mainly N substitutional doping give rise to band gap narrowing by mixing of N 2p (gray area) with O 2p states near the top of the valence band. This band gap narrowing enables the material to shift the optical absorption into visible light range. The oxynitride shows a computed band gap of extremely small value although experimentally the material is known to be semi-conducting. Qualitatively, the DOS plots are very different from those of pure oxide and nitrogen-doped oxide. Thus our computed comparative results are in line with experimental observations and clearly demonstrate that nitrogen doping is responsible for the band gap narrowing with respect to pure oxide material and hence responsible for red shift in optical absorption thereby making the material visible-light active photocatalyst. This idea is schematically depicted in figure 5 as a band model.

Anionic doping with N, C, or S atoms induces light absorption and photocatalytic activity in visible region. The top of valence band for doped-catalysts has major contribution from 2p orbitals of these elements causing band gap narrowing while the bottom of conduction band due to transition metal d orbitals remained almost unchanged. Yet, many nitrogen-doped materials derived from oxides are nonstoichiometric and contain oxygen defects probably due to the difference in the formal oxidation numbers of oxygen (−2) and nitrogen (−3). This may be the reason why the absorption spectra of nitrogen-doped materials are usually noisy or often show only shoulder in the visible light region with the main absorption edge still in the UV region. In any case, these defects will reduce the efficiency of the photocatalyst. Excessive nitrogen doping usually changes the structure to stoichiometric oxynitrides or nitrides and show clean red-shift of the absorption edges. Yet, in many cases, these stable phases are not active for the desired photocatalytic reactions, although there could be a few exceptions like TiON as discussed [32]. Finally there is a stability concern of the doped elements during long-term photocatalytic reactions.

5. New single-phase photocatalytic materials

Another approach to obtain visible light photocatalysts is to find new materials independent of UV-active materials. Undoped, single-phase oxide materials are of particular interest because of their intrinsic stability. There is only a handful of such materials reported recently including $BiVO_4$ [36], $RbPb_2Nb_3O_{10}$ [37], and $CaBi_2O_4$ [38]. The solid solution between a wide band gap semiconductor and a small band gap semiconductor could also belong to this group of new single phase materials, e.g. GaN–ZnO [39] and ZnS–$CuInS_2$–$AgInS_2$

[40]. We also reported a novel oxide photocatalyst, $PbBi_2Nb_2O_9$, an Aurivillius-phase perovskite, which is an efficient photocatalyst for water splitting into O_2 or H_2, isopropyl alcohol (IPA) degradation to CO_2, and production of photocurrent, all under visible light [41].

The UV–Visible diffuse reflectance spectrum for this compound is compared with that of nitrogen-doped TiO_2 ($TiO_{2-x}N_x$) in figure 6. From these spectra, we estimated the band gap energies of these materials as summarized in table 2. The $PbBi_2Nb_2O_9$ sample showed a single sharp edge in the visible light region, whereas $TiO_{2-x}N_x$ sample showed two absorption edges; the main edge due to the oxide at 390 nm and a shoulder due to the nitride at 451 nm. Both samples showed yellow color. The photocatalytic reduction of H_2O into H_2 and photocatalytic oxidation of H_2O into O_2 were performed under visible light ($\lambda \geq 420$ nm). Again, methanol and silver ion were used as scavengers of hole and photoelectron, respectively. The photocatalytic H_2 evolution over Pt-loaded $PbBi_2Nb_2O_9$ was observed, but the quantum yield was only ca. 0.95%. The quantum yield for O_2 evolution on $PbBi_2Nb_2O_9$ was estimated to be ca. 29%. This high quantum yield for O_2 formation is impressive and only TaON was reported to show a comparable quantum yield of 34% [32]. $TiO_{2-x}N_x$ showed a trace amount of H_2 evolution, but the quantum yield for O_2 evolution was as high as ca. 12%. The high quantum yield for O_2 formation indicates that the $PbBi_2Nb_2O_9$ has a high oxidation potential for photooxidation reaction under visible light irradiation. To exploit this high oxidation potential, oxidative decomposition of gaseous isopropyl alcohol (IPA) was tested. Under the same condition of visible light, the photocatalytic activity of $PbBi_2Nb_2O_9$ for IPA decomposition was about twice as high as that of $TiO_{2-x}N_x$.

The electronic band structure of $PbBi_2Nb_2O_9$ was calculated in figure 7. The conduction and valence bands of this compound consist of empty Nb 4d and occupied O 2p orbital, with the latter hybridized with Bi 6s and Pb 6s, giving the smaller band gap compared to compounds that do not contain Pb and Bi in its structure. Thus, the band gap energy of $PbBi_2Nb_2O_9$ was reduced to the visible light region by interaction of O 2p and Pb 6s/Bi 6s. Then, the visible light absorption takes place due to the transition from O 2p hybridized with Pb 6s/Bi 6s to Nb 4d. It is important to note that the visible light could be absorbed and induce both photocatalytic reduction and oxidation without any dopant for $PbBi_2Nb_2O_9$. Furthermore, nearly complete substitution of lead or bismuth into layered perovskites such as $CaBi_4Ti_4O_{15}$ (Aurivillius phase), $K_{0.3}La_{0.7}Ca_{1.7}Nb_3O_{10}$ (Dion–Jacobson phase), and $Sr_3Ti_2O_7$ (Ruddlesden–Popper phase) turned these UV-active layered perovskite photocatalysts into visible-light active photocatalysts ($PbBi_4Ti_4O_{15}$, $K_{0.2}La_{0.2}Bi_{0.6}Ca_{0.4}Pb_{0.8}Nb_3O_{10}$, and $Pb_3Ti_2O_7$) for water splitting [42]. The fact that those recent examples of reported single-phase oxide photocatalysts discussed above, i.e. $BiVO_4$ [36], $RbPb_2Nb_3O_{10}$ [37], and $CaBi_2O_4$ [38], also contain lead or bismuth does not appear to be just a coincidence.

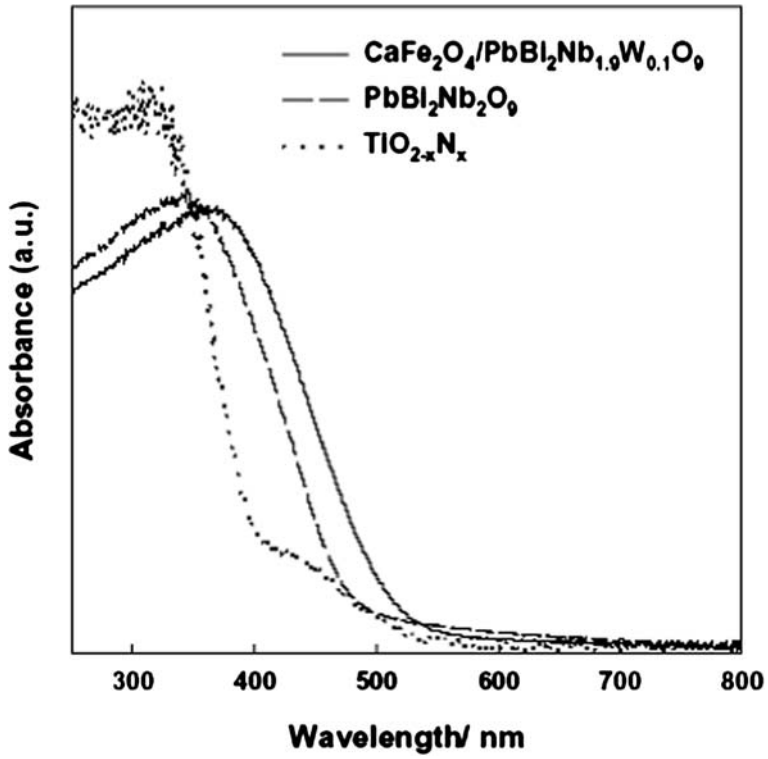

Figure 6. Optical transitions probed by UV–Vis spectroscopy for $CaFe_2O_4/PbBi_2Nb_{1.9}W_{0.1}O_9$, $PbBi_2Nb_2O_9$ and nitrogen-doped TiO_2.

Table 2
Band gap energies and photocatalytic activities for H_2 and O_2 evolution

Catalysts	Band gap energy		Hydrogen evolution		Oxygen evolution	
	E_g (eV)	λ_{ab} (nm)	μmol/gcat·hr	Q.Y. (%)	μmol/g cat h	Q.Y. (%)
$CaFe_2O_4/PbBi_2Nb_{1.9}W_{0.1}O_9$	2.75	450	34.8	4.2	675	38
$PbBi_2Nb_2O_9$	2.88	431	7.6	0.95	520	29
$CaFe_2O_4$	1.99	623	Trace	0	Trace	0
$TiO_{2-x}N_x$	2.77	451	Trace	0	221	14

Catalyst loaded with 0.1 wt% Pt, 0.3 g; light source, 450 W W-Arc lamp(Oriel) with UV cut-off filter(λ≥420 nm). Reaction was performed in aqueous methanol solution for H_2 generation (methanol 30 ml + distilled water 170 ml) or in an aqueous $AgNO_3$ solution for O_2 generation (0.05 mol/l, 200 ml).

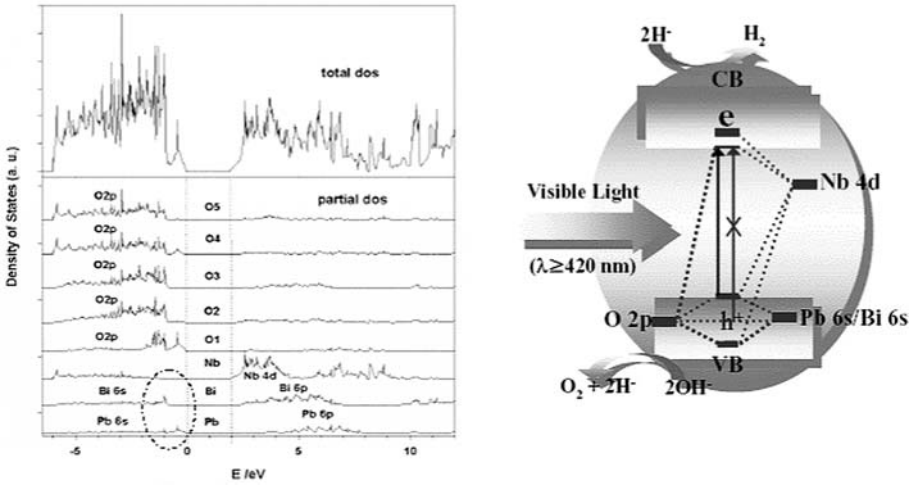

Figure 7. Calculated total and projected density of states of $PbBi_2Nb_2O_9$ and its band structure model. The band gap energy of $PbBi_2Nb_2O_9$ was reduced by interaction of O 2p and Pb 6s/Bi 6s and the visible light absorption takes place due to the transition from O 2p hybridized with Pb 6s/Bi 6s to Nb 4d.

Thus substitution of lead or bismuth could be a generic method of visible light sensitization of wide band gap oxide materials in general.

6. Multi-component photocatalysts

As discussed, photocatalysts for PWS should satisfy the stringent requirements of both band gap energy and band positions. When a single component photocatalyst cannot meet these requirements, employment of multi-component photocatalysts could become an alternative. There are number of ways to combine the functions of different materials (i) to simply mix an oxidation-type photocatalyst and a reduction-type photocatalyst in a solution containing a redox couple as an electron shuttle, e.g. WO_3/Cr, Ta-doped $SrTiO_3$ in I^-/IO_3^- solution [43], (ii) to intercalate nanoparticles of a photocatalyst into the layers of the other semiconductor, e.g. CdS/$HNb(Ta)WO_6$ [44] or $Fe_2O_3/HTiNb(Ta)O_5$ [45], and (iii) to couple two semiconductors with different band positions for efficient and longer charge separation, e.g. CdS–TiO_2 [46]. We describe here a novel configuration of composite solids, designated as photocatalytic nanodiode (PCD), that comprises of nano-islands of p-type $CaFe_2O_4$ interfaced over highly crystalline layered perovskite base lattice (n-type $PbBi_2Nb_{1.9}W_{0.1}O_9$), yielding nano-dimensional p–n junctions [47].

It has been demonstrated in photovoltaic cells and photoelectrochemical (PEC) cells that diode structures made of n- and p-type semiconductors show greatly enhanced activities compared to the devices consisting of a single semiconductor. For example, the fundamental unit of current silicon solar cells is made of p–n junction of p-type and n-type silicon. Multi-junction solar cells and PEC cells of remarkable energy conversion efficiencies have been reported [48]. Nozik constructed an n-TiO_2/p-GaP diode electrode for a PEC cell, which was found to be much more active than either n-TiO_2 or p-GaP single-component electrode for the decomposition of water [49]. He designated his monolithic device a p–n type photochemical diode. We attempted to create a particulate version of the p–n junction in nanometer scale for photocatalytic applications, which should be stable under typical photocatalytic reaction conditions and highly active under visible light. Noting the employment of p–n junction concept,

nano-scale size, and particulate form of our device material, we designated it a p–n type photocatalytic nanodiode (PCD).

We employed $PbBi_2Nb_2O_9$ [39] discussed above as the suitable n-type semiconductor. In order to render it n-type semiconductivity, the material was doped with hexavalent tungsten W^{VI} to obtain n-$PbBi_2Nb_{1.9}W_{0.1}O_9$. In addition to the valency, the similarity of its size (0.74 nm) to that of Nb^V (0.78 nm) was also considered in the choice of tungsten dopant. $CaFe_2O_4$ is a p-type metal oxide semiconductor with the bulk band gap of 1.9 eV as shown earlier [50]. In order to combine these two semiconductor particles to form a p–n junction, we devised the configuration of the diode particles; (i) nanocrystals of p-type $CaFe_2O_4$ and (ii) perovskite lattice of n-type $PbBi_2Nb_{1.9}W_{0.1}O_9$ as submicron-sized base material. Thus, $CaFe_2O_4$ nanoparticles and $PbBi_2Nb_{1.9}W_{0.1}O_9$ submicron particles were synthesized individually by sol–gel and solid-state reaction methods, respectively. Then, produced individual components were combined by putting them into hydrothermal reactor (150 °C for 7 days) to obtain $CaFe_2O_4$ nano-islands formed over larger particles of $PbBi_2Nb_{1.9}W_{0.1}O_9$.

Figure 8a shows HRTEM of a typical PCD particle that clearly exhibits the existence of nano-islands dispersed over a single particle of perovskite base-material. The micrograph shows many nano-crystalline islands of 5–10 nm and the magnified view of a nano-island reveals the nano-crystallinity of $CaFe_2O_4$. The magnified view of fringes also demonstrates the existence of highly crystalline, layered base material with the layer thickness of 0.4 nm corresponding to $PbBi_2Nb_{1.9}W_{0.1}O_9$. The phase identification was also confirmed by elemental analysis with *in situ* energy-dispersive X-ray microanalysis carried out during the microscopic study. Based on these experimental observations we proposed a schematic model for PCD as illustrated in figure 8b**.** Each island forms a nano-scale p–n junction at the interface that has a crucial role in the photocatalytic process. The working principle of PND is schematically shown as an energy band model for one p–n junction (figure 8c), in which the energy scale is drawn according to the flat-band potential measurements. At thermal equilibrium, the Fermi levels of two semiconductors align. When the device is immersed in an electrolyte, the band edges of the conduction and valence bands bend as indicated. The operation of PCD is initiated by the absorption of the band gap photons in both the n- and p-type semiconductors. Photo-generated holes and electrons separate under the influence of electric field corresponding to energy diagram shown in figure 8c. Thus holes move to p-$CaFe_2O_4$ side and electrons to n-$PbBi_2Nb_{1.9}W_{0.1}O_9$ side. Thus the net effect of the p–n diode formation is the efficient separation of electron–hole pairs to minimize the energy-wasteful electron–hole recombination. This effect will lead to the higher photocatalytic activity.

The UV–Visible diffuse reflectance spectrum and the estimated band gap energy are shown in figure 6 and table 2 together with those of the base material, $PbBi_2Nb_2O_9$ and nitrogen-doped TiO_2. The PCD powders showed a steep onset of absorption spectrum near around green wavelength sweeping major visible region and showed orange color. We studied photodecomposition of water in the presence of sacrificial agents. For these reactions, two reference catalysts were loaded with 0.1 wt% Pt as a co-catalyst to collect photo-electrons away from holes by forming a Schottky-type junction structure. As listed in table 2, PCD demonstrated the best performance even without any co-catalyst. The quantum yield of O_2 evolution (4×the number of

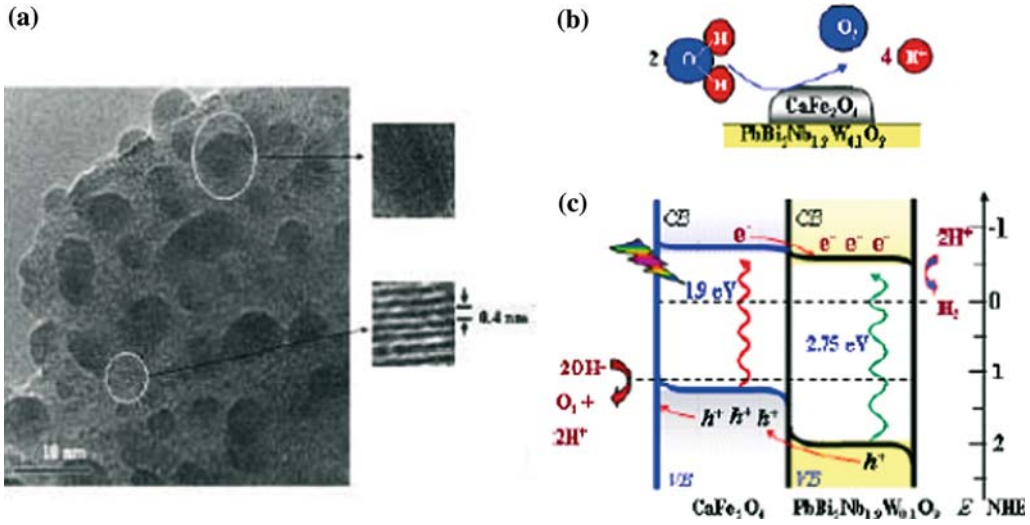

Figure 8. Proposed photocatalytic nanodiode (PCD) consisting of p-type $CaFe_2O_4$ and n-type $PbBi_2Nb_{1.9}W_{0.1}O_9$ base perovskite. (a) HRTEM of the fabricated PCD showing the nanocrystalline p-$CaFe_2O_4$ interfaced on the layers of n-$PbBi_2Nb_{1.9}W_{0.1}O_9$ base. (b) Schematic of one *PCD* working for water oxidation; (c) Schematic energy band model of a PCD showing the formation of p–n junction and the process of water oxidation. The band positions were derived from flat band potential measurements.

generated O_2 molecules/the number of absorbed photon) over PCD was estimated to be ca. 38%. To the best of our knowledge, this is the highest value ever reported for the reaction over semiconductor photocatalysts under visible light. The hydrogen evolution with methanol as a hole scavenger was slower, yet PCD showed a respectable quantum yield of ca. 4.2%. The rate of IPA decomposition also increased by a factor of ca. 4 compared with that over $PbBi_2Nb_2O_9$.

It has been demonstrated that the photocatalytic p–n nanodiode (PCD) comprising of nano-islands of p-type $CaFe_2O_4$ interfaced over highly crystalline layered-perovskite base-lattice (n-type $PbBi_2Nb_{1.9}W_{0.1}O_9$), is a highly active novel photocatalyst. Application of the p–n diode concept commonly employed in monolithic energy conversion devices and employment of nano materials synthesis techniques, have allowed the fabrication of a nanocomposite between the high-order oxides with a unique configuration. It appears that the p–n diode formation results in the efficient separation of electron–hole pairs to minimize the energy-wasteful electron–hole recombination, which leads to the high photocatalytic activity.

7. Summary and perspective

In this article, we have summarized our efforts to fabricate active photocatalysts that could split water under visible light with the ultimate goal to utilize the sunlight as the primary energy source of hydrogen production. At the moment, our results as well as those of other laboratories show still low efficiencies of light-to-hydrogen conversion. Furthermore, the most of the results (except Ref. [26] and [45]) are for half reactions that produce only either hydrogen or oxygen in the presence of sacrificial agents. These agents scavenge electrons or holes in an irreversible manner making the process unsustainable. Yet, if we run the PWS reaction in the PEC mode, these half reactions can take place separately at each electrode. Thus photocatalysts showing high activities in the half reactions could be employed in PEC systems as one of electrodes. Then, the greatest remaining challenge should be the low efficiency of light utilization. Finding new photocatalytic materials with unique structure and phase is still likely to be the key to the success. High throughput screening or combinatorial chemistry approaches as well as more rational search based on fundamental calculations/predictions should be useful. In addition, the synthesis of these materials with high crystallinity and high surface area is also important, because these properties exert great impact on the activity of the material of the same structure and phase. Finally, smart combination and modification of known materials could also be fruitful. The research on PWS is evolving rapidly. Considering the time that PWS under UV light took from the initial demonstration in 1972 to today's highly efficient photocatalysts with quantum yields as high as 50%, there is no reason that we cannot expect similar speed of development in the visible-light active photocatalysis as well. Then, technically and economically viable visible-light photocatalysts for PWS could be available in a near future.

Acknowledgment

This work was supported by National Research Laboratories Program, Hydrogen Energy Center, General Motors R& D Center, and National R&D Project for Nano Science and Technology.

References

[1] A. Fujishima and K. Honda, Nature 238 (1972) 37(London).
[2] K. Domen, A. Kudo and T. Onishi, J. Catal. 102 (1986) 92.
[3] Y. Inoue, Y. Asai and K. Sato, J. Chem. Soc., Faraday Trans. 909 (1994) 797.
[4] A. Kudo and H. Kato, Chem. Lett. (1997) 867.
[5] H.G. Kim, D.W. Hwang, J. Kim, Y.G. Kim and J.S. Lee, Chem. Commun. (1999) 1077.
[6] V. Reddy, D.W. Hwang and J.S. Lee, Catal. Lett. 90 (2003) 39.
[7] D.W. Hwang, J. Kim and J.S. Lee, Catal. Lett. 80 (2002) 53.
[8] D.W. Hwang, H.G. Kim, J. Kim, K.Y. Cha, Y.G. Kim and J.S. Lee, J. Catal. 193 (2000) 40.
[9] J. Kim, D.W. Hwang, S.W. Bae, Y.G. Kim and J.S. Lee, Korean J. Chem. Eng. 18 (2001) 941.
[10] J. Kim, D.W. Hwang, H.G. Kim, S.W. Bae and S.M. J.S. Ji Lee, Chem. Commun. (2002) 2488.
[11] D.W. Hwang, J.S. Lee, W. Li and S.H. Oh, J. Phys. Chem. B. 107 (2003) 4963.
[12] H.G. Kim, D.W. Hwang, S.W. Bae and J.S. Lee, Catal. Lett. 91 (2003) 193.
[13] J. Kim, D.W. Hwang, H.G. Kim, J.S. Lee, W. Li and S.H. Oh, Topics Catal. (2005) 35.
[14] K. Sayama, A. Tanaka, K. Domen, K. Maruya and T. Onishi, J. Catal. 124 (1990) 541.
[15] K. Sayama, H. Arakawa and K. Domen, Catal. Today 28 (1996) 175.
[16] N. Ishizawa, F. Marimo, T. Kawamura and M. Kimura, Acta. Crystallogr. Sect. B 31 (1975) 1972.
[17] K. Domen, M. Hara, J.N. Kondo, T. Takata, A. Kudo, H. Kobayashi and Y. Inoue, Korean J. Chem. Eng. 18 (2001) 862.
[18] A. Kudo, Catal. Surveys Asia 7 (2003) 31.
[19] T. Sakata, in *Photocatalysis, Fundamentals and Applications*, N. Serpone and E. Pelizzetti (eds), (Wiley, New York, 1989).
[20] M. Koca and M. Sahin, Int. J. Hydrogen Energy 27 (2002) 363.
[21] J. Wu, J.M. Lin, Y.B. Shu and T. Sato, J. Mater Chem. 11 (2001) 3343.
[22] B. O'Regan and M. Grätzel, Nature 353 (1991) 737.
[23] E. Borgarello, J. Kiwi, M. Grätzel, E. Pelizzetti and M. Visca, J. Am. Chem. Soc. 104 (1982) 2996.
[24] H. Yamashita, M. Harada, J. Misaka, M. Takeuchi, K. Ikeue and M. Anpo, J. Photochem. Photobiol. A 148 (2002) 257.
[25] H. Kato and A. Kudo, J. Phys. Chem. B 106 (2002) 5029.
[26] Z. Zou, J. K. Ye Sayama and H. Arakawa, Nature 414 (2001) 625.
[27] D.W. Hwang, H.G. Kim, J.S. Lee, W. Li and S.H. Oh, J. Phys. Chem. B 109 (2005) 2093.
[28] D.W. Hwang, H.G. Kim, J.S. Jang, S.W. Bae, S.M. Ji and J.S. Lee, Catal. Today 93 (2004) 845.

[29] D.W. Hwang, K.Y. Cha, J. Kim, H.G. Kim, S.W. Bae and J.S. Lee, Ind. Eng. Chem. 42 (2003) 1184.
[30] R. Asahi, T. Morikawa, T. Ohwaki, K. Aoki and Y. Taga, Science 293 (2001) 269.
[31] S.U.M. Khan, M. Al-Shahry, W.B. Ingler Jr and , Science 297 (2002) 2243.
[32] G. Hitoki, T. Takata, J.N. Kondo, M. Hara, H. Kobayashi and K. Domen, Chem. Commun. (2002) 1698.
[33] A. Kasahara, K. Nukumizu, G. Hitoki, T. Takata, J.N. Kondo, M. Hara, H. Kobayashi and K. Domen, J. Phys. Chem. A 106 (2002) 6750.
[34] A. Kasahara, K. Nukumizu, T. Takata, J.N. Kondo, M. Hara, H. Kobayashi and K. Domen, J. Phys. Chem. B 107 (2003) 791.
[35] S.M. Ji, P.H. Borse, H.G. Kim, D.W. Hwang, J.S. Jang, S.W. Bae and J.S. Lee, Phys. Chem. Chem. Phys. 7 (2005) 1315.
[36] A. Kudo, K. Omori and H. Kato, J. Am. Chem. Soc. 121 (1999) 11459.
[37] Y. Yoshimura, Y. Ebina, J. Kondo, K. Domen and A. Tanaka, J. Phys. Chem. 97 (1993) 1970.
[38] J. Tang, Z. Zou and J. Ye, Angew. Chem. Int. Ed. 43 (2004) 4463.
[39] K. Maeda, T. Takada, M. Hara, N. Saito, Y. Inoue, H. Kobayashi, K. Domen, J. Am. Chem. Soc. 127 (2005) 8286.
[40] I. Tsuji, H. Kato, A. Kudo and Angew, Chem. Int. Ed. 44 (2005) 3565.
[41] H.G. Kim, D.W Hwang and J.S Lee, J. Am. Chem. Soc. 126 (2004) 8912.
[42] H.G. Kim, O.S. Becker, J.S. Jang, P.H. Borse and J.S. Lee, J. Solid State Chem. in press.
[43] K. Sayama, K. Mukasa, R. Abe, Y. Abe and H. Arakawa, J. Photochem. Photobiol. A 148 (2002) 71.
[44.] J. Wu, S. Uchida, Y. Fujishiro, S. Yin and T. Sata, J. Mater. Chem. 11 (2001) 3343.
[45] J.S. Jang, H.G. Kim, V.R. Reddy, S.W. Bae, S.N. Ji and J.S. Lee, J. Catal. 231 (2005) 213.
[46] N. Serpone, E. Borgarello and M. Grätzel, J. Chem. Soc. Chem. Commun. (1983) 42.
[47] H.G. Kim, P.H. Borse, W. Choi and J.S. Lee, Angew. Chem. Int. Ed. 44 (2005) 4565.
[48] O. Khaselev and J. Turner, Science 280 (1998) 425.
[49] A.J. Nojik, Appl. Phy. Lett. 29 (1976) 150.
[50] Y. Matsumoto, J. Sol. Stat. Chem. 126 (1996) 227.